

Effect of “TMCP/Accelerated Cooling” parameters on the microstructure and mechanical properties of 40 mm thick sheets of X70 steel grade produced from heavy slabs

Vadym Zurnadzy^{1,2*}, Yuliia Chabak^{1,2}, Ivan Petryshynets², Vasily Efremenko^{1,2,3},
Michail Brykov⁴, Alexey Efremenko¹, Ruslan Sagirov⁵, Taras Kovbasiuk⁶

¹*Pryazovskyi State Technical University, 4944 Dnipro, Ukraine*

²*Institute of Materials Research, Slovak Academy of Sciences, 04001 Kosice, Slovak Republic*

³*International Research Institute for Steel Technology, Wuhan University of Science and Technology, 430081 Wuhan, P. R. China*

⁴*National University Zaporizhzhia Polytechnic, 69063 Zaporizhzhia, Ukraine*

⁵*Metallurgical Plant Kametstal, 51900 Kamians'ke, Ukraine*

⁶*Lviv Polytechnic National University, 79000 Lviv, Ukraine*

Received 25 May 2024, received in revised form 1 October 2024, accepted 2 December 2024

Abstract

The effects of thermo-mechanical controlled processing (TMCP) and accelerated cooling (AC) on the structure and mechanical properties of 40 mm thick sheets of X70 steel made of heavy slabs (300 mm thick) are studied in this work. A TMCP with a rolling finish in a two-phase temperature interval followed by AC to 480–530 °C was found optimal, ensuring full compliance with the API X70 grade in tensile and Charpy tests, while the result of a drop weight tear test (DWTT) at –20 °C was close to the standard level. This was due to the formation of fine-grained quasi-polygonal/acicular ferrite strengthened by the martensite/austenite islands and nanosized (Nb,V)C precipitates. The advanced combination of mechanical properties in 40 mm thick sheets refers to using slabs of increased thickness, allowing sufficient rolling reduction to refine a cast structure of the billet effectively. The DWTT fractures concerning steel microstructure are discussed.

Key words: pil/gas pipe, X70 steel grade, thermo-mechanical controlled processing (TMCP), accelerated cooling, microstructure, mechanical properties

1. Introduction

The current development of the oil/gas industry requires constructing new pipelines of increased pressure and throughput to improve transportation efficiency [1–3]. Using up-to-date high-strength pipeline steel with advanced mechanical properties is feasible to meet this challenge. 97 % of oil and natural gas transportation pipelines are produced from hot-rolled steel coils [4]. The principal international standard regulating steel pipe quality is an American Petroleum Institute Specification 5L (API 5L) [4, 5]. This standard proposes several steel grades from X42 to X120, where the numbers indicate the strength measured in pounds per square inch. Using high-strength steel

allows for cutting the prices of pipeline construction due to reduced logistic costs and decreased pipe wall thickness [5]. However, steel of X100 and X120 grades remain to be of future applications; at present, X70 and X80 grades are the most reputable and most often used by pipeline operators due to their excellent combination of strength, sub-zero impact toughness, H₂S-corrosion resistance, and weldability [13]. The technology of X70 steel sheets production has been optimized and improved, making this material successfully used for several decades in constructing offshore infrastructure and pipelines, including for an arctic environment [4, 6, 7]. According to API 5L (PSL2), the yield tensile strength (YTS) and ultimate tensile strength (UTS) of grade X70 should be within 485–

*Corresponding author: e-mail address: vadim.zurnadzy@gmail.com

Table 1. Chemical composition (wt.%) of the steels studied

| Steel | C | Mn | Si | Nb | V | Cr | Ni | Cu | Ti | Mo | Al | S |
|-------|------|------|------|-------|-------|------|------|------|-------|------|------|-------|
| A | 0.06 | 1.59 | 0.25 | 0.058 | 0.022 | 0.16 | 0.29 | 0.23 | 0.012 | 0.07 | 0.02 | 0.002 |
| B | 0.07 | 1.60 | 0.25 | 0.048 | 0.048 | 0.11 | 0.27 | 0.16 | 0.014 | 0.07 | 0.02 | 0.002 |

635 MPa and 570–760 MPa, respectively. The ductility of X70 steel is controlled by the values of total elongation (TEL, $\geq 22\%$) and absorbed impact energy (E) under the Charpy V-notch test (CVNT, ≥ 54 J). Also, the drop weight tear test (DWTT) is applied to evaluate the fracture propagation in specimens with an actual pipeline wall thickness. The indicative DWTT criterion is $\geq 85\%$ of a ductile fracture (shear area – SA) (known as the “Battelle 85% SA criterion” [8, 9]). Though CVNT and DWTT are conducted at zero centigrade (API 5L), the testing temperature may be subzero per the customer’s request.

Currently, two main processing routes have been used to achieve the X70 grade level, namely the heat treatment (HT) (including conventional quenching and tempering [10–12]) and the thermo-mechanical controlled process (TMCP) [13–16]. The TMCP is widely used since it allows for acquiring targeted mechanical properties without HT, thus cutting technological costs [17–19]. During TMCP, two main parameters are controlled: (a) the temperature ranges of rough and finishing rolling and (b) the corresponding reduction ratio [20, 21]. The TMCP is often followed by accelerated cooling (AC) at special cooling equipment [22–24] to additionally improve the strength and reduce the structural banding [3, 25, 26]. The effect of TMCP/AC parameters on the mechanical properties of a pipeline of the X70/X80 grades is extensively studied in [12–16, 18, 22, 27, 28], aiming at providing the required properties through the phase-structural state regulation. The welding of X70/X80 steel under pipe production may deteriorate its properties; therefore, the study of the heat-affected zone and post-welding heat treatment are also interesting to researchers [29–32].

It is worth noting that the published works are primarily focused on the pipe sheets of lower thickness (up to 25–30 mm) produced from slabs of a standard thickness (220–270 mm) [33–35]. However, steel sheets of increased thickness (35–40 mm) for thick-wall pipelines of underwater or high-pressure applications [37, 41] are also in demand. As the sheet thickness increases, it becomes more difficult to meet the X70 requirements. When the thick sheets are produced from the standard slab, deformation does not sufficiently “elaborate” the axial zone. Accordingly, the thru-thickness chemical and structural inhomogeneity in the sheet cannot be improved enough, which is detrimental to ductility and subzero fracture propagation [36, 37]. This is especially relevant for DWTT, in which the size factor is crucial [8, 38–40]: the thicker

the plate, the lower the DWTT results. Therefore, the thick slabs are needed to get the appropriate rolling reduction when producing the thick sheets. The literature contains limited works dedicated to the TMCP regimes intended to produce 35–40 mm thick steel sheets rolled from heavy thick slabs. This work aimed to study the effect of the TMCP/AC parameters on the mechanical properties of the 40 mm-thick steel of X70 API 5L (PSL2) manufactured from slabs of increased thickness (300 mm). With that, additional attention was paid to the sub-zero fracture behavior of the steel, which is important for its further applications.

2. Materials and methods

The research material was the 40 mm-thick sheets of X70 grade steel. The sheets were hot-rolled from the 300-thick mm slabs. The steels containing 0.06–0.07 wt.% C, of two different alloying combinations were used (Table 1). Steel A had a higher amount of the elements (Cr, Ni, Cu, Mo) which retard the pearlite transformation [15, 26, 42] (total amount of these elements were 0.75 wt.% (steel A) and 0.61 wt.% (steel B)). In turn, steel B possessed an increased amount of strong carbide-forming elements (Nb, V, Ti) (with a total amount of 0.092 wt.% (steel A) and 0.110 wt.% (steel B)). Steel was smelted in the oxygen steel-making converter and poured into the slabs using a continuous casting machine.

Before rolling, the 300 mm-thick slabs were soaked at 1180–1200 °C for 5 hours. Rough rolling was carried out according to a two-stage scheme (Fig. 1). The first (preliminary) stage of rough rolling was stopped at 1040–1060 °C when the slab was reduced to 135–140 mm. Then, it was cooled in the air to 910–930 °C and rolled to a thickness of 10–112 mm (the 2nd stage of rough rolling). Under the finishing stage, the steel was eventually rolled by several passes to 40 mm. The finish rolling was conducted by two schedules: (a) start at 880–900 °C and finish at 820–840 °C (Fig. 1a), (b) start at 820–840 °C and finish at 760–770 °C (Fig. 1b). Critical temperature A_{r3} was found by Choquet’s equation [43] (Eq. (1)) as follows:

$$A_{r3}(\text{°C}) = 902 - 527 \cdot C - 62 \cdot \text{Mn} + 60 \cdot \text{Si}, \quad (1)$$

where C, Mn, and Si are the contents of chemical elements (wt.%).

The A_{r3} temperatures for steel A and B were calcu-

Table 2. The regimes and parameters of a TMCP/AC process. T_{RF} is the temperature of the rolling finish. For T_{ACF} and C_R , the target and experimental (in parentheses) values are given

| Regime number | T_{RF} (°C) | T_{ACS} (°C) | T_{ACF} (°C) | C_R (°C s ⁻¹) |
|---------------|---------------|----------------|----------------|-----------------------------|
| Schedule 1 | | | | |
| 1-1 | 820–840 | 790–810 | 600 (600–620) | 15 (12.9–14.8) |
| 1-2 | | | 550 (545–556) | 15 (15.9–16.3) |
| 1-3 | | | 500 (496) | 15 (17.4) |
| Schedule 2 | | | | |
| 2-1 | 760–770 | 735–755 | 550 (560–585) | 20 (17.0) |
| 2-2 | | | 500 (475–535) | 20 (20.6–22.2) |
| 2-3 | | | 450 (450–460) | 20 (22.0–23.0) |
| 2-4 | | | < 450 | 20 (21.8–23.0) |

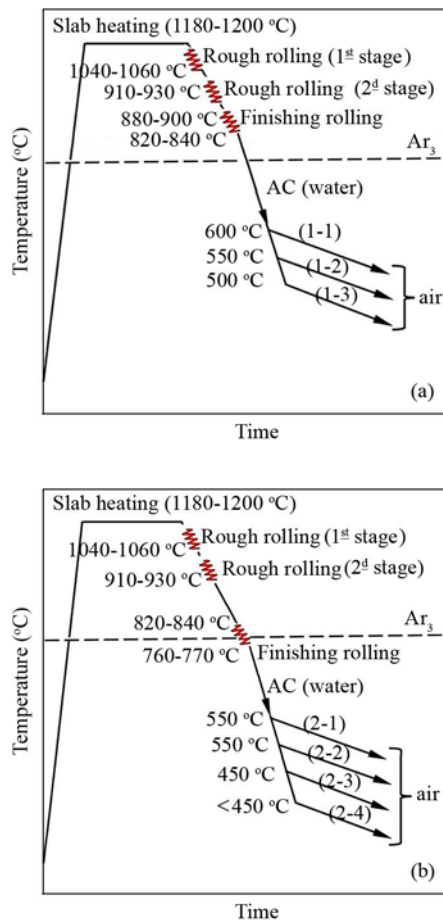


Fig. 1. Schematic diagram of TMCP process: (a) schedule 1 (regimes (1-1)–(1-3)) and (b) schedule 2 (regimes (2-1)–(2-4)).

lated as 787 and 781 °C, respectively. Accordingly, the finish rolling was stopped in a single-phase (austenite) interval (Fig. 1a) or the upper part of a two-phase (austenite + ferrite) interval (Fig. 1b).

After the rolling completion, the rolled sheets were cooled by water jets in the accelerated cooling unit. The parameters of AC regimes are depicted in Table 2. The latter include temperature of cooling start (T_{ACS}), temperature of accelerated cooling finish (T_{ACF}), and cooling rate (C_R). One sheet 6000 mm long and 2000 mm wide was used for processing by each TMCP/AC regime presented in Table 2. The cooling rate was estimated automatically based on the pyrometric measurements of the sheet surface along its centreline [44]. After the AC finished, the sheets were collected in a stack, where they slowly cooled in the air to 100 °C for 40 hours.

Tensile tests were conducted at room temperature according to ISO 6892-1:2019, using cylindrical specimens with a 10 mm-diameter gauge under a 0.1 mm s⁻¹ strain. The absorbed impact energy was measured at -20 °C using the Charpy method using a pendulum tester and V-notched specimens of 10 × 10 × 55 (mm³) size. According to APL regulations, the specimens were extracted by cutting from the plate in a longitudinal direction at a depth of L of thickness. To get the average value, three tensile and three V-notched specimens were used for each experimental regime. Drop weight tear test (one specimen for each regime) was carried out on the press-notched transverse-longitudinal specimens of 76 × 305 × b (mm³) in size. The specimens of a full sheet thickness ($b = 40$ mm) were tested at -20 °C; the specimens machined (milled) from both sides to a thickness of $b = 19$ mm were tested at a lower temperature (-37 °C). The optical microscope “Axiovert 40 MAT” (Carl Zeiss) and scanning electron microscope (SEM) “Ultra-55” (Carl Zeiss) were utilized for the microstructure characterization of the mirror-polished specimens after etching by the 4 vol.% Nital reagent. Also, the mentioned SEM was used to observe the fracture surface. The ferrite grain size and the degree of structural banding were measured under ASTM E112-13 and ASTM E1268-19, respectively. The fine struc-

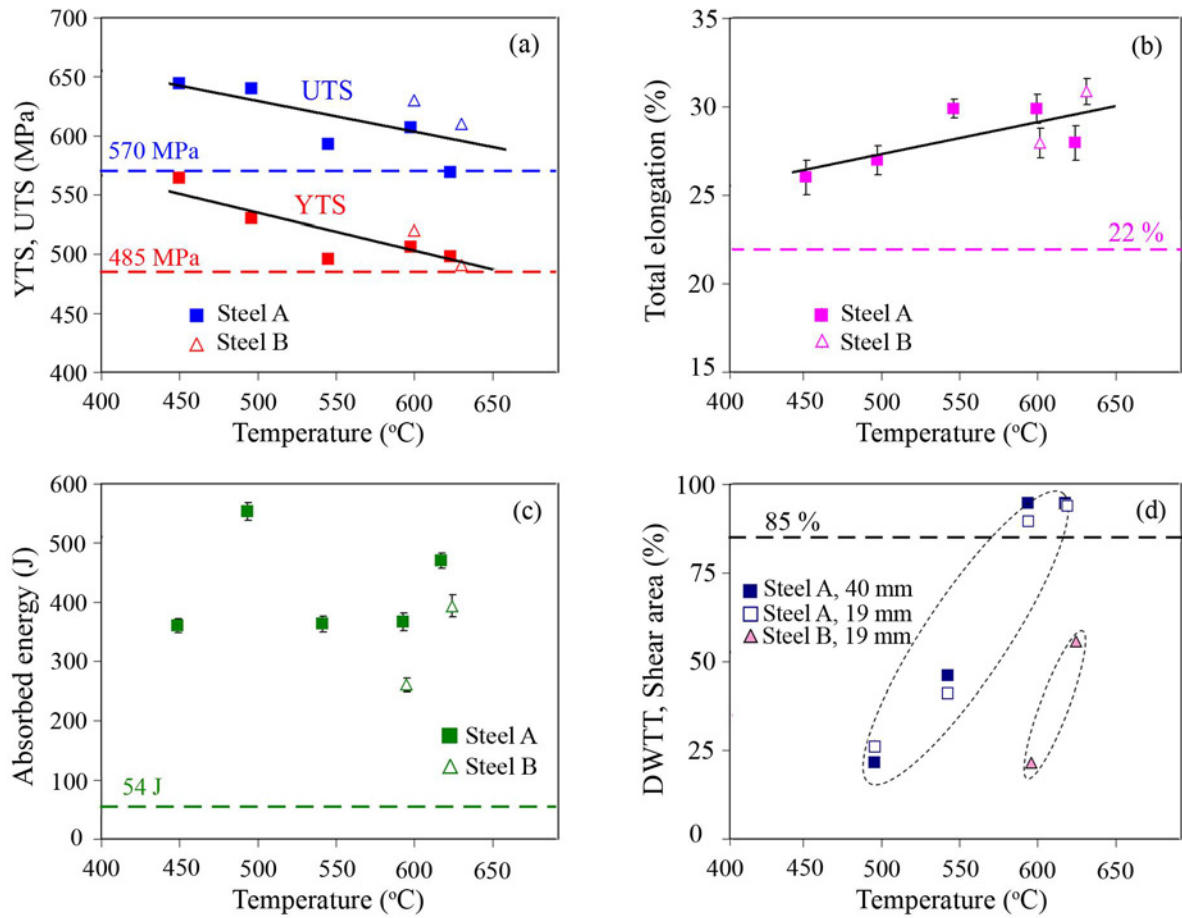


Fig. 2. The effect of the T_{ACF} under accelerated cooling from the single-phase region (schedule 1) on the mechanical properties of 40 mm-thick sheets (the dotted line indicates the requirements of APL X70 grade).

ture of the steel was studied employing the transmission electron microscopy (TEM) “JEM-100-C-XII” (JEOL) at 100 kV acceleration voltage. For TEM investigation, thin foils were mechanically polished to about 0.1 mm thickness, followed by electro-polishing in 6-vol.% $HClO_4$ solution using a fluid-jet polishing installation.

3. Results and discussion

3.1. TMCP/AC with a rolling finish in a single-phase temperature interval

Figure 2 presents the mechanical properties of 40 mm-thick steel sheets after TMCP/AC according to the regimes (1–1)–(1–3) (schedule 1). Under these regimes, the water cooling was started when steel was in a single-phase (austenitic) structural state. The obtained values of YTS and UTS varied in the range of 491–564 MPa and 570–640 MPa, correspondingly ensuring full compliance with X70 grade requirements for the steel strength (Fig. 2a). Moreover, the YTS/UTS ratio varied in the range of 0.81–0.88 also

meeting the standard requirements (≤ 0.90). As seen in Fig. 2a, there is a low-angle slope tendency of increasing YTS and UTS with a decrease in T_{ACF} . The experimental data for both steels fit well into the general dependencies described by the following equations:

$$YTS \text{ (MPa)} = -0.32T_{ACF} + 693.48, \quad (2)$$

$$UTS \text{ (MPa)} = -0.26T_{ACF} + 760.21. \quad (3)$$

The opposite tendency was revealed for total elongation, the values of which (27–31 %) significantly exceeded the X70 level (Fig. 2b):

$$TEL \text{ (%) } = 0.020T_{ACF} + 18.06. \quad (4)$$

An even greater excess over the specified standard level was recorded for absorbed impact energy, which varied in the range of 330–60 J (Fig. 2c). It is noteworthy that this advanced impact behavior was demonstrated under sub-zero testing (-20°C), i.e., at more severe conditions than the standard requirements (0°C). Unlike YTS, UTS, and TEL, the ab-

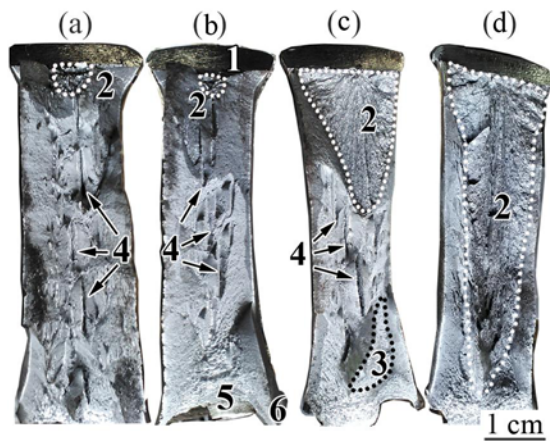


Fig. 3. Fracture surface of DWTT specimens after a TMCP/AC treatment (schedule 1) with a T_{ACF} of (a) 623 °C (steel A), (b) 598 °C (steel A), (c) 545 °C (steel A), and (d) 600 °C (steel B). All the specimens are of 19 mm thickness, tested at -37 °C. (1 – a notch, 2 – a “cleavage area”, 3 – an “inverse fracture area”, 4 – a separation (delamination), 5 – a hammer impact area, 6 – a “shear lip”).

sorbed impact energy was not dependent on the T_{ACF} .

The DWTT results are presented in Fig. 2d as an SA fraction measured on the fractured surface of the specimen. The areas of a brittle fracture comprised the “cleavage area” (initiated by the notch) and the “inverse fracture area” caused by the strain hardening under the hammer impact [38, 45]. As follows from Fig. 2d, the DWTT behavior met the standard requirements ($SA \geq 85\%$) only in steel A and after accelerated cooling to T_{ACF} of 600–620 °C. In this case, the specimen’s fractured surface exhibited ductile rupture (SA of 95 %) with a minor fraction of the cleavage zone (depicted by the dotted line) and numerous separations (Figs. 3a,b). The shear area was characterized by the ductile relief consisting of multiple dimples (Fig. 4a). The separations were the delamination areas associated with the crystallographic textures $\langle 110 \rangle \{001\}$ and $\langle 100 \rangle \{001\}$ caused by the TMCP process [46]. The DWTT separations are considered [47] an important indicator showing that the crack deflected during its propagation, thus hindering the brittle fracture manifestation (as seen in Fig. 3c, the separations were associated specifically with the ductile area). With a T_{ACF} decrease, the SA of steel A dropped to $\leq 50\%$ for both “full-thickness” and the “19 mm-thick” specimens, indicating the negligible effect of a size factor [46]. In these cases, the DWTT specimens performed mostly brittle cleavage fracture with the flat facets of a “river” [48] pattern (Fig. 4b). Steel B manifested even more brittle DWTT behavior, showing SA of 20–55 % at $T_{ACF} = 600$ –630 °C, despite of reduced samples thickness (Fig. 3d).

The images of the corresponding microstructure of

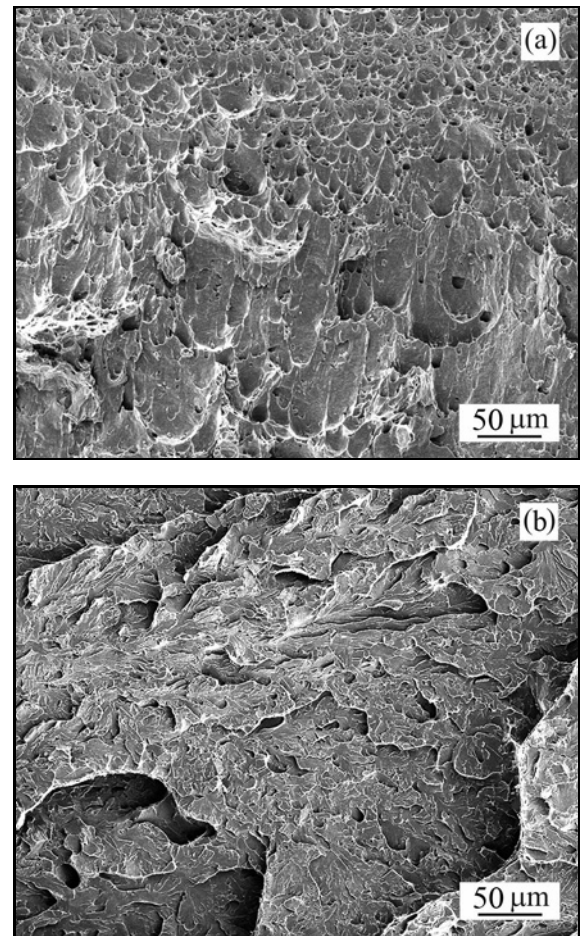


Fig. 4. The pattern of a fractured surface of DWTT specimens made of (a) a shear area (steel A, T_{ACF} of 598 °C) and (b) a cleavage area (steel B, T_{ACF} of 600 °C).

steels are illustrated in Fig. 5. Under accelerated cooling from austenite region to T_{ACF} of 600–630 °C with a lower cooling rate (12.9 – 14.8 °C s^{-1}) (regime 1–1), a ferrite-pearlite banded structure was formed in steel A featuring a ferrite grain of 9–8 numbers and a banding of 1–3 degrees. In this structure, the ferrite was present in both polygonal and quasi-polygonal forms, while pearlite emerged both as individual colonies and discontinuous stripes (Fig. 5a). Such structure ensured high DWTT performance (SA of 95 %), excellent absorbed energy, and good TEL; however, it provided a YTS at minimally acceptable for X70 grade level only. Decreasing T_{ACF} to 550 °C (regime 1-2) allowed to significantly reduce the pearlite volume fraction which remained as small isolated areas; also, the polygonal ferrite was replaced with finer (10–11 numbers) quasi-polygonal/acicular ferrite (Fig. 5b). Within the ferrite grains the occasional fine carbide precipitates (of 34–50 nm in diameter) were revealed (shown by the arrows in Fig. 5c). Further decrease in TCF to 500 °C (with CR of 17.4 °C s^{-1}) mostly inhibited pearlite for-

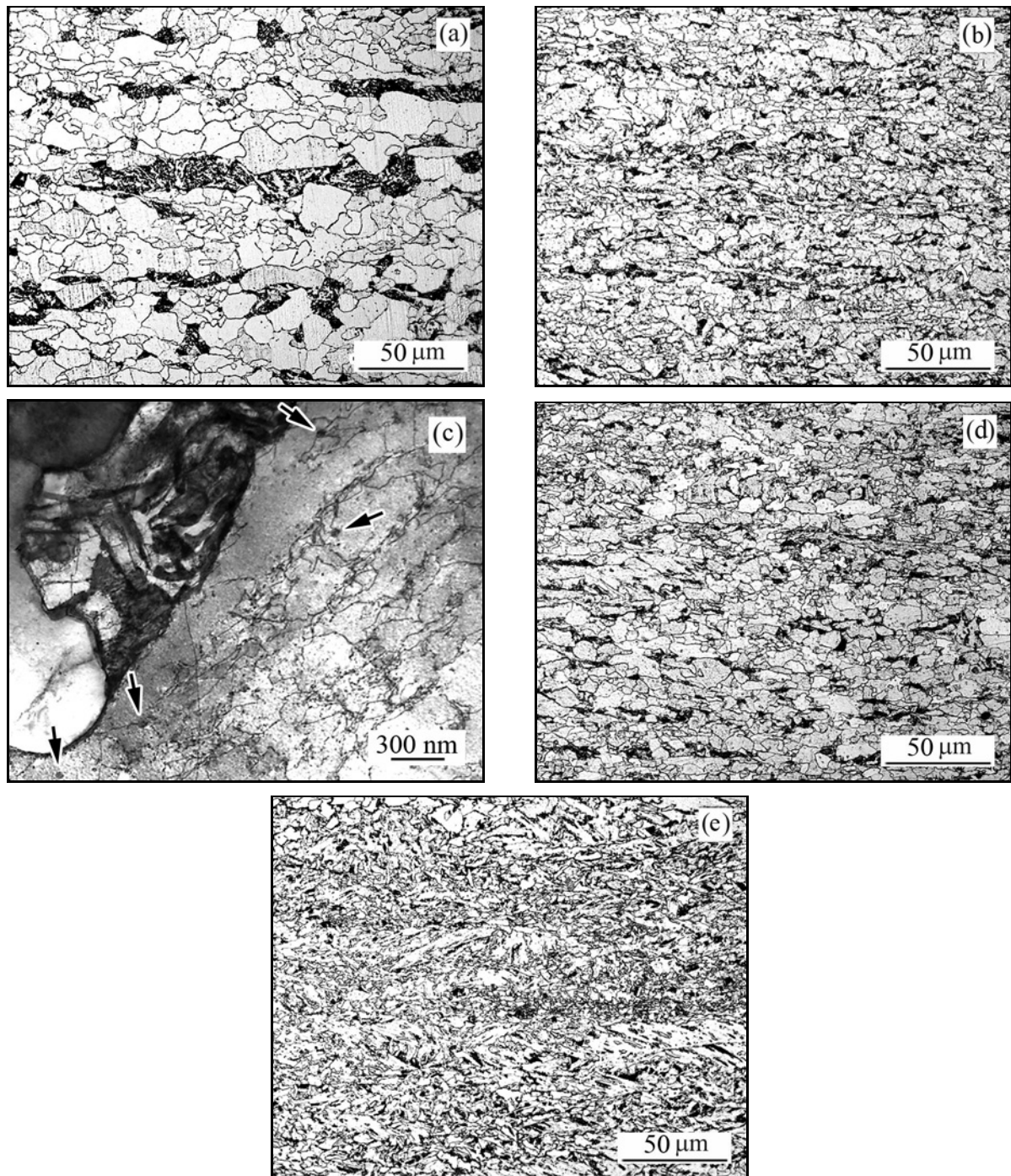


Fig. 5. Microstructure specimens of steel A ((a), (b), (c), and (e)) and steel B (d) after a TMCP/AC treatment (schedule 1) with a T_{ACF} of (a) 630°C, (b, e) 550°C, (c) 500°C, (d) 600°C ((a), (b),(d), and (e) – OM images; (c) – TEM image).

mation and resulted in quasi-polygonal/acicular ferrite with a dispersed martensite-austenite “islands” (Fig. 5c). Regimes (1–2) and (1–3) ensured the structure without structural banding thus promoting a moderate increase in strength and advanced absorbed energy (up to 500 J). With that, the shear area at DWTT was dramatically reduced to 20–45%. The treatment of steel B with a T_{ACF} of 630°C (regime

1–1) resulted in a ferrite-pearlite structure (similar to steel A), though with coarser ferrite grains (of 8-9 numbers, ASTM E112-13). The coarse grains affected DWTT, which decreased to an unsatisfactory level (SA of 55%). At T_{ACF} of 600°C, in contrast to steel A, a bainitic (acicular ferrite) structure was formed in steel B (Fig. 5d), which caused the sharp increase in brittle fracture in the DWTT specimen (SA of 20%).

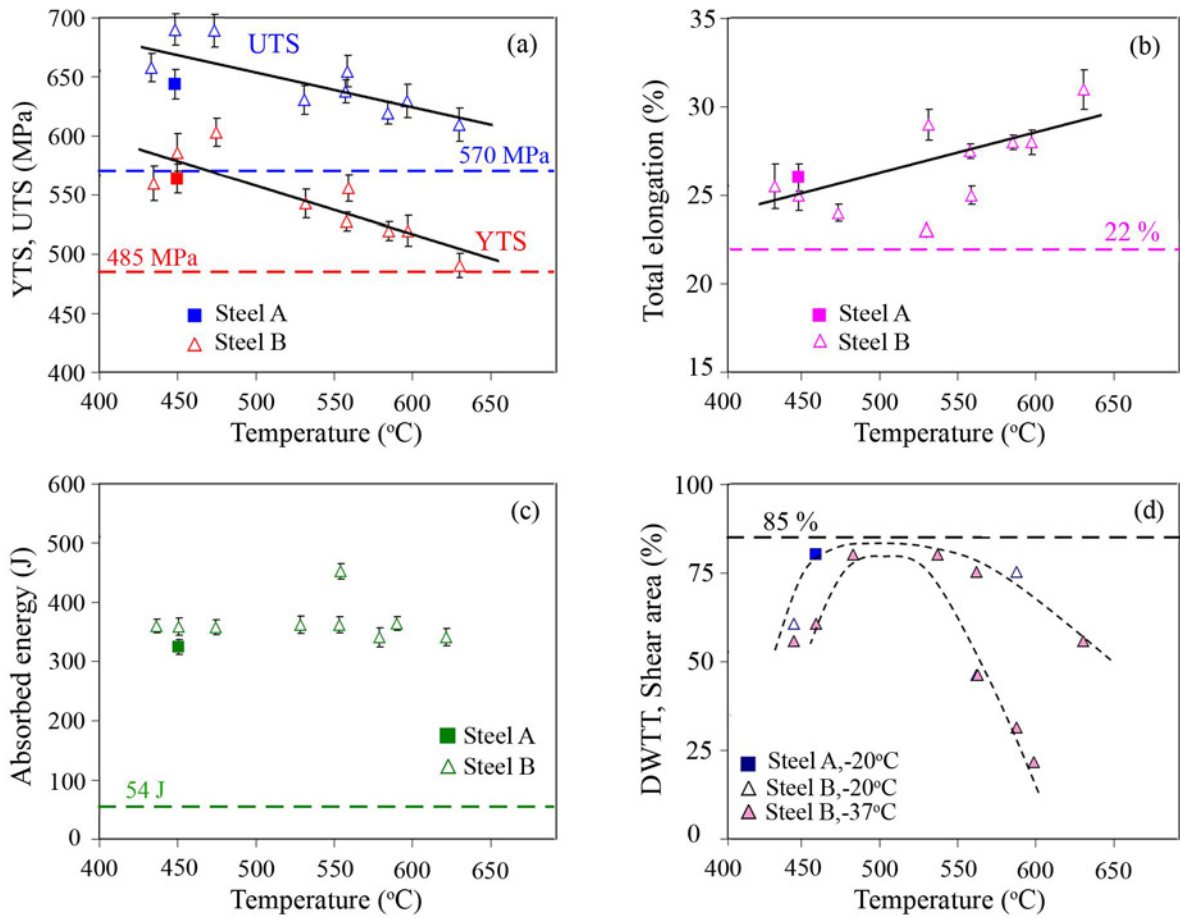


Fig. 6. The effect of the T_{ACF} under accelerated cooling from the two-phase region on the mechanical properties of 40 mm-thick sheets (the dotted line indicates the requirements of APL X70 grade).

3.2. TMCP/AC with a rolling finish in a two-phase temperature interval

Figure 6 depicts the mechanical properties of steel B after the accelerated cooling by the regimes (2-1)–(2-4). These regimes refer to cooling from an “austenite + ferrite” temperature domain while the cooling rate was higher as compared with the regimes (1-1)–(1-3). The results showed that for all regimes, the results of tensile and impact tests fully complied with the standard requirements. With that, under the regime (2-1), when cooling finishes in the region of pearlite transformation (600–630 °C), the strength indicators (YTS, UTS) were at the minimal standard level. Under cooling from the two-phase region, the dependencies of YTS and UTS on the temperature of the cooling finish have a steeper slope (Fig. 6a), i.e., higher strength values were achieved as compared with the regimes (1-1)–(1-3). For TEL, the same dependence was observed as for regimes (1-1)–(1-3) being directly proportional to T_{ACF} (Fig. 6b). The variations of YTS, UTS, and TEL depending on T_{ACF} (°C) are described as follows:

$$YTS \text{ (MPa)} = -0.41T_{ACF} + 762.76, \quad (5)$$

$$UTS \text{ (MPa)} = -0.29T_{ACF} + 801.90, \quad (6)$$

$$TEL \text{ (\%)} = 0.023T_{ACF} + 14.58. \quad (7)$$

In contrast to accelerated cooling from the austenitic region, the sub-zero absorbed energy performed negligible scatter: most values were within the range of 350–400 J, exceeding the standard requirements by about 7 times (Fig. 6c). No dependence of absorbed energy on T_{ACF} was observed. As shown in Fig. 6d, the DWTT exhibited a significantly different profile as to cooling from a “single-phase” temperature domain: the SA values varied non-monotonically, with a maximum corresponding to T_{ACF} of 475–530 °C. In this case, the SA values reached 80 %, slightly inferior to the APL X70 requirements. No substantial differences were noticed in the DWTT results concerning such testing features as specimen thickness and temperature.

The microstructures of the specimens cooled from the “austenite + ferrite” temperature interval are pre-

sented in Fig. 7. When accelerated cooling stopped at a relatively high temperature ($\geq 550^\circ\text{C}$), the transformation proceeded by the pearlite mechanism with the formation of a ferrite-pearlite structure consisting of quasi-polygonal/polygonal ferrite (grain of 9–8 numbers) and pearlite bands (with banding of 1–2 degrees) (Fig. 7a). At lower T_{ACF} (475–535 $^\circ\text{C}$), the dif-

fusion (pearlitic) transformation was significantly inhibited being replaced by shear-based transformation. Accordingly, pearlite mostly vanished in the structure (just occasional grainy pearlite colonies retained) while polygonal ferrite was substituted by fine-grained (grain number of 10) quasi-polygonal or acicular ferrite (Fig. 7b). Also, the islands of martensite/austenite

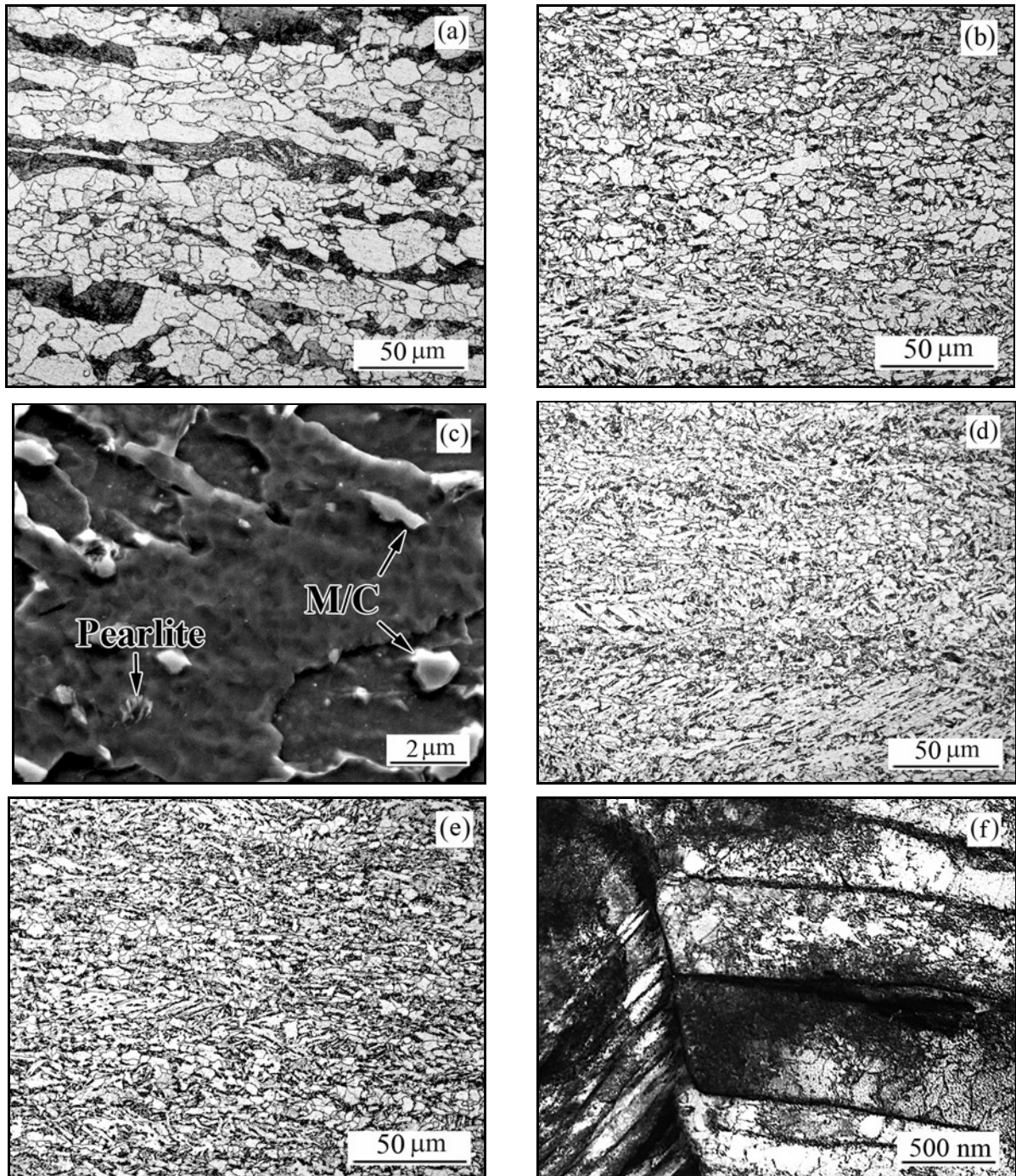


Fig. 7a–f. Microstructure of steel B, after accelerated cooling from the two-phase region (schedule 2) to T_{ACF} of: (a) 560–585 $^\circ\text{C}$; (b), (c) 475–535 $^\circ\text{C}$; (d) 450–460 $^\circ\text{C}$; (e), (f) $\leq 450^\circ\text{C}$ ((a), (b), (d), and (e) – OM images; (c) – SEM image; (f) – TEM image).

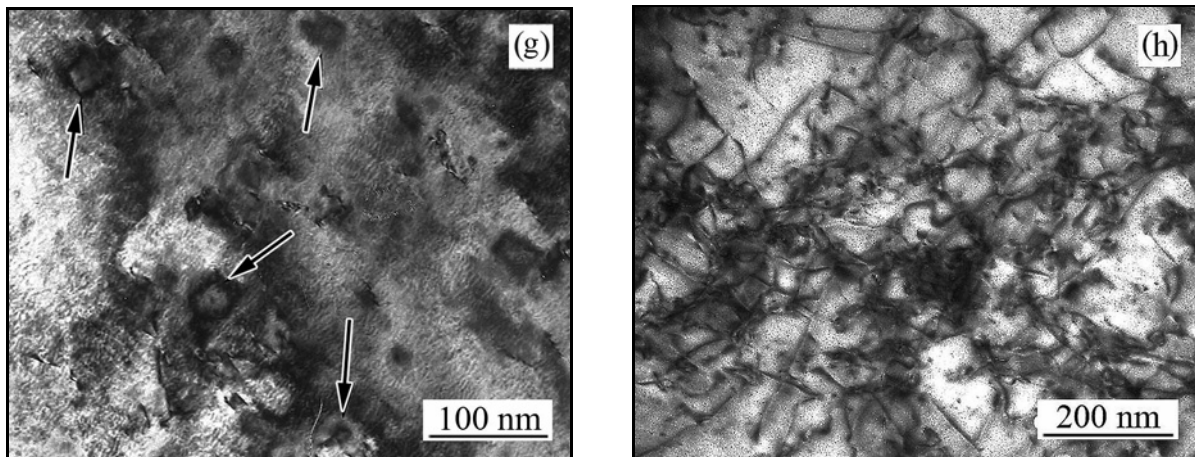


Fig. 7g,h. Microstructure of steel B, after accelerated cooling from the two-phase region (schedule 2) to T_{ACF} of: (g) and (h) 450–460 °C, TEM images).

conglomerates appeared in the structure (Fig. 7c). Such structure corresponded to the maximum DWTT results (Fig. 6d). Under cooling to ≤ 450 °C, the steel acquired the quasi-polygonal ferrite/bainite structure (Figs. 7d,e), which increased strength (YTS, UTS) but negatively affected TEL and DWTT. Bainite was characterized by an increased density of dislocations (Fig. 7f). In the steel treated by the regimes of schedule 2, the nanosized carbide precipitates (shown by the arrows in Fig. 7g) were revealed within the ferrite grains (laths). The precipitates interacted with the sliding dislocation by the Orowan mechanism, forming a “dislocation forest” (Fig. 7h), effectively blocking the slip systems, thus increasing strength.

The studies have shown that in rolled steel sheets of a higher thickness (40 mm), it is possible to meet the requirements of X70 grade in mechanical properties (except DWTT tested at -20 °C). That was due to the increased thickness of the slab (300 mm), which ensured a deeper deformation-based refinement of the cast structure. When producing 40 mm thick sheets from the slabs of a conventional thickness (220–270 mm), the reduction ratio is 5.5–6.7. Using thicker slabs (300 mm) ensured an increased ion ratio to 7.5, i.e., by 12–36 %, leading to more deep deformation and eliminating dendritic structure and segregations in the axis zones. The thru-thickness refinement and chemical homogenization were beneficial for ductility, especially for absorbing impact energy that performed at an extraordinary level under subzero (-20 °C) testing. The advanced combination of strength, ductility, and impact toughness was ensured by consecutive usage of TMCP and accelerated water cooling, which allowed the synergy of the strain accumulation with the pearlite-free structure (acicular ferrite) of increased strength. The strain-induced work hardening depends on the recrystallization behavior (also referred to as “softening mechanisms” [49]), which is determined by the non-recrystallization temperature (T_{nr}): at the

temperatures below T_{nr} , the recrystallization and recovery are fully inhibited leading to “pancaking” (flattening) of the austenite grains [18]. T_{nr} can be found by Boratto’s equation [50]:

$$T_{nr}(\text{°C}) = 887 + 464C + (6445\text{Nb} - 644(\text{Nb})^{-0.5}) + (732V - 230(V)^{-0.5}) + 890\text{Ti} + 363\text{Al} - 357\text{Si}, \quad (8)$$

where C, Nb, V, Ti, Al, and Si are the element contents (wt.%).

The T_{nr} was calculated as 1044.2 and 1002.9 °C for steel A and B, respectively. The high position of T_{nr} in steels A and B is due to strain-induced NbC precipitation, which proceeds under rolling at temperatures ≤ 1050 °C [51], in both sheets of steel sheets stage of rough rolling and finishing rolling proceeded via Type II No-recrystallization [49], leading to strain accumulation in austenite. The latter transformed into fine-grained ferrite with an increased dislocation density, promoting a strength increase [20, 22, 25]. However, the distinction in the temperature regime of finish rolling caused differences in the properties level after accelerated cooling (Fig. 8). Schedule 2 provided the higher strength relative to schedule 1, as illustrated in Fig. 8a by comparison of average linear dependencies of YTS and UTS on T_{ACF} temperature. As T_{ACF} decreased, the advantage of schedule 2 in the yield strength increased from 11 MPa at 650 °C to 29 MPa at 450 °C. The difference in UTS values depends to a lesser extent on T_{ACF} , amounting to 22 MPa at 650 °C and 29 MPa at 450 °C. The increase in strength was a trade-off by a slight deterioration in plasticity after schedule 2, as average TEL decreased by 1.5 points at 650 °C and 2.1 points at 450 °C (Fig. 8b). As for CVNT, schedule 2 provided a slightly lower (by 30.7 J) mean value of absorbed energy while the maximum scatter of the values decreased 2.2 times compared to schedule 1 (Figs. 2c and 6c).

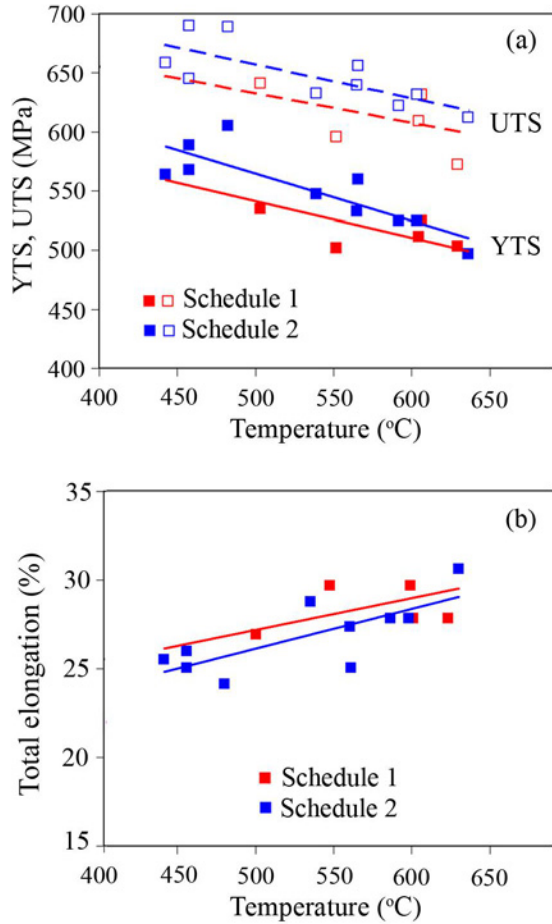


Fig. 8. “Mechanical property – T_{ACF} ” correlations for different TMCP/AC schedules: (a) YTS and UTS, and (b) total elongation.

The described change in properties occurred since, in the case of schedule 2, the temperature of the rolling finish was shifted to the two-phase ($\gamma + \alpha$) region. The presumptive reasons for the strength increase are as follows: (i) under the finishing rolling, an “austenite ferrite” transformation proceeded; hence, ferrite was also strained and dislocation-hardened [52], and (ii) the strain-induced carbide (Nb,V)C precipitation from ferrite took place [25]. As reported by Klinkenberg et al. [51], the reason (ii) was enabled by retaining part of niobium in the solution after NbC precipitation in the austenite temperature domain. The equilibrium solubility of niobium in ferrite is inversely proportional to temperature (Eq. (1)) that causes the precipitation of (Nb,V)C from ferrite under the plate cooling [51]:

$$\log K_{NbC}^{\alpha-Fe} = \frac{11030}{T} + 4.90, \quad (9)$$

K is the equilibrium constant, and T is the temperature (in Kelvin).

The precipitation hardening can be evaluated us-

ing the Ashby-Orowan equation [53]:

$$\Delta\sigma_{DP} = \frac{6.66}{L} \ln \frac{D}{4.96 \times 10^{-4}}, \quad (10)$$

where D is the mean planar intercept diameter of a precipitate and L is the surface-to-surface precipitate spacing, which is found as [54]:

$$L = D \left[\left(\frac{\pi}{4f} \right)^{0.5} - 1 \right], \quad (11)$$

where f is the volume fraction of the precipitates.

Parameters D and f were derived from the TEM images (Fig. 7g) to be 12.5 ± 0.25 nm and 0.45 vol.%, respectively. The strengthening of precipitation was calculated as 24.1 MPa. This value is compatible with the difference in YTS between schedules 1 and 2 (Fig. 8a), proving the above assumption about the reason for an advantage of schedule 2 in strength. When deformation finishes at relatively high temperatures (schedule 1), coarse inclusions of carbide NbC are formed (Fig. 5c), which does not contribute to the strength of the steel [55].

The completion of accelerated cooling at ~ 480 – 530 °C is considered the optimal regime since it provides a promising combination of mechanical properties (YTS of 540–580 MPa, UTS of 630–660 MPa, TEL of 24–27 %, $E_{-20^\circ C}$ of 350–400 J), while DWTT at -20 °C (SA of 80 %) was close to that of the target level (85 %). Remarkably, all the properties were achieved by the steel sheets, which increased to 40 mm thickness.

As follows from Fig. 2, $DWTT_{-20^\circ C}$ reached the required level only after TMCP/AC treatment with T_{AFC} of 600–620 °C (SA of 95 %), where a banded ferrite/pearlite structure was formed (this regime did not fully meet the X70 strength requirements). That allows the conclusion that the banded structure benefits the DWTT behavior owing to the texture induced by the TMCP process [45] and due to the band interface acting as a “barrier” for crack propagation. Notably, the separations (associated with a TMCP texture [44, 45]) were observed only on the ductile fracture surface, indicating the advantage of a banded texturized structure under the DWTT conditions. A gradual decrease in the T_{AFC} resulted in a replacement of pearlite with stronger acicular ferrite, leading to the banding elimination and a drastic decrease in DWTT results (under the rolling finish in a single-phase temperature domain). When AC was conducted from the two-phase temperature domain, the banding elimination at T_{ACF} of ~ 480 – 530 °C, in contrast, increased the DWTT results that can be attributed to the specific structure of fine-grained quasi-polygonal/acicular ferrite strengthened by the M/A islands and the disperse carbide precipitates.

The present studies show the feasibility of using heavy slabs of increased thickness to produce steel sheets intended for thick-wall oil-gas pipelines of the X70 grade. The direction of further research is to optimize the chemical composition of the steel to improve the subzero behavior under the DWTT conditions.

4. Conclusions

This work investigated the microstructure and mechanical properties of 40 mm thick sheets of low-carbon (0.06–0.07 wt.% C) (Cr, Ni, Mo, V, Nb)-microalloyed steel, produced from heavy slab to comply with the requirements of X70 (API 5L) grade. Based on the obtained results, the major conclusions are drawn as follows:

1. Applying a heavy slab of increased thickness is found to be feasible to produce thick (≥ 30 mm) steel sheets intended for oil/gas pipelines. Using a 300 mm thick slab allowed for an increase in rolling reduction by 12–36 % when producing 40 mm thick sheets, which enabled better deformation to eliminate the cast structure in the axis zone of the billet. This resulted in structure refining, which enhanced low-temperature impact behaviors (Charpy V-notch test, DWTT) of steel, ensuring compliance with an X70 (API 5L) grade.

2. The sheets were produced through the three-stage thermo-mechanical controlled processing (TMCP) with a rolling finish in a single-phase interval (820–840 °C) or in a two-phase interval (760–780 °C) followed by accelerated cooling (AC). For both TMCP schedules, the decrease in temperature of AC finish (T_{ACF}) from 630 to 450 °C led to a gradual increase in strength indicators (YTS, UTS) and a decrease in ductility (TEL). The low temperature (–20 °C) impact behavior was not dependent on TACF presenting exceptional absorbed energy, which reached maximally 550 J.

3. The optimal combination of the mechanical properties (YTS of 540–580 MPa, UTS of 630–660 MPa, TEL of 24–27 %, subzero absorbed energy of 350–400 J, subzero DWTT (shear area) of 80 %) was attributed to the TMCP with rolling finish in “austenite + ferrite” interval followed by accelerated water cooling (20–23 °C s^{–1}) to T_{ACF} of 480–530 °C. These properties were ensured by forming a microstructure consisting of a fine-grained quasi-polygonal/acicular ferrite, the martensite/austenite islands, and the nanosized carbide precipitates. The earlier stop of water cooling (at 600–630 °C) resulted in a banded “ferrite + pearlite” structure with lower YTS, which barely met the requirements of X70 grade.

4. The highest DWTT level (SA of 95 %) referred to the “ferrite + pearlite” structure obtained by TMCP with a rolling finish in a single-phase interval.

In the case of rolling finish in a two-phase interval, the best DWTT results (SA of 80 %) were attributed to the structure of quasi-polygonal/acicular ferrite. Bainite formation under a later AC finish (at ≤ 450 °C) resulted in a drastic decrease in DWTT behavior.

5. TMCP/AC processing with a rolling finish in a two-phase interval had an advantage in YTS and UTS at any T_{ACF} . This behavior is presumably attributed to the nanosized (12.5 ± 0.25 nm) (Nb,V)C particles precipitated during the “austenite \rightarrow ferrite” transformation. The dispersion hardening is evaluated as 24.1 MPa, which is compatible with the difference in strength between the two TMCP schedules.

Acknowledgements

This research was funded by the Ministry of Education and Science of Ukraine (project No. 0123U100374) and National Research Foundation of Ukraine (project No. 2021.01/0189). Yu. Chabak, V. Efremenko and I. Petryshynets appreciate the support of Slovak Research and Development Agency in the frame of the project APVV-23-0341.

References

- [1] J. Y. Yoo, S. S. Ahn, D. H. Seo, W. H. Song, K. B. Kang, New development of high grade X80 to X120 pipeline steels, *Mater. Manuf. Processes* 26 (2011) 154–160. <https://doi.org/10.1080/10426910903202534>
- [2] S. K. Sharma, S. Maheshwari, A review on welding of high strength oil and gas pipeline steels, *J. Nat. Gas Sci. Eng.* 38 (2017) 203–217. <https://doi.org/10.1016/j.jngse.2016.12.039>
- [3] L. Z. Xu, G. Y. Qiao, X. Gong, Y. Gu, K. Xu, F. R. Xiao, Effect of through-thickness microstructure inhomogeneity on mechanical properties and strain hardening behavior in heavy-wall X70 pipeline steels, *J. Mater. Res. Technol.* 25 (2023) 4216–4230. <https://doi.org/10.1016/j.jmrt.2023.06.198>
- [4] Ş. O. Turhan, A. Motameni, R. Gürbüz, Fatigue behavior of welded API 5L X70 steel used in pipelines, *J. Fail. Anal. Prev.* 20 (2020) 1554–1567. <https://doi.org/10.1007/s11668-020-00959-x>
- [5] M. Witek, Possibilities of using X80, X100, X120 high-strength steels for onshore gas transmission pipelines, *J. Nat. Gas Sci. Eng.* 27 (2015) 374–384. <https://doi.org/10.1016/j.jngse.2015.08.074>
- [6] S. I. Lee, S. Y. Lee, S. G. Lee, H. G. Jung, B. Hwang, Effect of strain aging on tensile behavior and properties of API X60, X70, and X80 pipeline steels, *Met. Mater. Int.* 24 (2018) 1221–1231. <https://doi.org/10.1007/s12540-018-0173-9>
- [7] R. K. Z. Davani, E. G. Ohaeri, S. Yadav, J. A. Szpunar, J. Su, M. Gaudet, M. Rashid, M. Arafin, Crystallographic texture and the mechanical properties of API 5L X70 pipeline steel designated for an arctic environment, *Mater. Sci. Eng. A* 889 (2024) 145849. <https://doi.org/10.1016/j.msea.2023.145849>

- [8] S. Y. Shin, B. Hwang, S. Lee, K. B. Kang, Effects of notch shape and specimen thickness on drop weight tear test properties of API X70 and X80 line-pipe steels, *Metall. Mater. Trans. A* 38 (2007) 537–551. <https://doi.org/10.1007/s11661-006-9073-6>
- [9] B. Hwang, S. Lee, Y. M. Kim, N. J. Kim, Correlation of rolling condition, microstructure, and low-temperature toughness of X70 pipeline steels, *Metall. Mater. Trans. A* 36A (2005) 1793–1805. <https://doi.org/10.1007/s11661-005-0043-1>
- [10] L. B. Godefroid, B. M. Sena, V. B. D. Trindade, Evaluation of microstructure and mechanical properties of seamless steel pipes API 5L type obtained by different processes of heat treatments, *Mater. Res.* 20 (2017) 514–522. <https://doi.org/10.1590/1980-5373-mr-2016-0545>
- [11] V. I. Zurnadzhy, V. G. Efremenko, K. M. Wu, I. Petryshynets, K. Shimizu, A. M. Zusin, M. N. Brykov, V. A. Andilakhai, Tailoring strength/ductility combination in 2.5 wt.% Si-alloyed middle carbon steel produced by the two-step Q-P treatment with a prolonged partitioning stage, *Mater. Sci. Eng. A* 791 (2020) 139721. <https://doi.org/10.1016/j.msea.2020.139721>
- [12] G. Mandal, S. K. Ghosh, S. Chatterjee, Effects of TMCP and QT on microstructure and properties of ultrahigh strength steel, *Mater. Today: Proc.* 18 (2019) 5196–5201. <https://doi.org/10.1016/j.matpr.2019.07.519>
- [13] O. Kurpe, V. Kukhar, E. Klimov, A. Prysiashnyi, Thermomechanical controlled rolling of hot coils of steel grade S355MC at the wide-strip rolling mill 1700, *Solid State Phenomena* 291 (2019) 63–71. <https://doi.org/10.4028/www.scientific.net/SSP.291.63>
- [14] A. Nowotnik, T. Siwecki, The effect of TMCP parameters on the microstructure and mechanical properties of Ti-Nb microalloyed steel, *J. Microsc.* 237 (2010) 258–262. <https://doi.org/10.1111/j.1365-2818.2009.03238.x>
- [15] J. Hu, L. X. Du, H. Xie, X. H. Gao, R. D. K. Misra, Microstructure and mechanical properties of TMCP heavy plate microalloyed steel, *Mater. Sci. Eng. A* 607 (2014) 122–131. <https://doi.org/10.1016/j.msea.2014.03.133>
- [16] L. Costa, G. Melo, N. Castro, A. Buschinelli, Microstructural characterization of API 5L X65 and X70 steels manufactured by TMCP process, *Tecnol. Metal. Mater. Min.* 19 (2022) e2511. <http://dx.doi.org/10.4322/2176-1523.20222511>
- [17] R. Parthiban, S. G. Chowdhury, K. C. Harikumar, S. Sankaran, Evolution of microstructure and its influence on tensile properties in thermo-mechanically controlled processed (TMCP) quench and partition (Q&P) steel, *Mater. Sci. Eng. A* 705 (2017) 376–384. <https://doi.org/10.1016/j.msea.2017.08.095>
- [18] A. Roccisano, S. Nafisi, D. Stalheim, R. Ghomashchi, Effect of TMCP rolling schedules on the microstructure and performance of X70 steel, *Mater. Character.* 178 (2021) 111207. <https://doi.org/10.1016/j.matchar.2021.111207>
- [19] V. Schwinn, J. Bauer, P. Flüß, H. J. Kirsch, E. Amoris, Recent developments and applications of TMCP steel plates, *Metall. Res. Technol.* 108 (2011) 283–294. <https://doi.org/10.1051/metal/2011054>
- [20] Y. Liu, F. Zhu, Y. Li, G. Wang, Effect of TMCP parameters on the microstructure and properties of an Nb-Ti microalloyed steel, *ISIJ Int.* 45 (2005) 851–857. <https://doi.org/10.1111/j.1365-2818.2009.03238.x>
- [21] X. D. Huo, L. J. Li, Z. W. Peng, S. J. Chen, Effects of TMCP schedule on precipitation, microstructure and properties of Ti-microalloyed high strength steel, *J. Iron Steel Res. Int.* 23 (2016) 593–601. [https://doi.org/10.1016/S1006-706X\(16\)30093-0](https://doi.org/10.1016/S1006-706X(16)30093-0)
- [22] W. Cai, Y.-B. Wang, G. Q. Li, R. Stroetmann, Comparative study on strength of TMCP and QT high-strength steel butt-welded joints, *J. Constr. Steel Res.* 197 (2022) 107447. <https://doi.org/10.1016/j.jcsr.2022.107447>
- [23] J. Zhao, W. Hu, X. Wang, J. Kang, G. Yuan, H. Di, R. D. K. Misra, Effect of microstructure on the crack propagation behavior of microalloyed 560MPa (X80) strip during ultra-fast cooling, *Mater. Sci. Eng. A* 666 (2016) 214–224. <https://doi.org/10.1016/j.msea.2016.04.073>
- [24] V. G. Efremenko, E. S. Popov, S. O. Kuzmin, O. I. Trufanova, A. V. Efremenko, Introduction of three-stage thermal hardening technology for large diameter grinding balls, *Metallurgist* 57 (2014) 849–854. <https://doi.org/10.1007/s11015-014-9812-7>
- [25] P. P. Singh, S. Mula, S. Ghosh, Grain refinement, strain hardening and fracture in thermomechanically processed ultra-strong microalloyed steel, *Mater. Today Commun.* 38 (2023) 107582. <https://doi.org/10.1016/j.mtcomm.2023.107582>
- [26] I. M. Andreiko, V. V. Kulyk, O. P. Ostash, Resistance of steels of railroad wheels to corrosion-fatigue fracture, *Materials Science* 47 (2012) 608–612. <https://doi.org/10.1007/s11003-012-9434-9>
- [27] S. Zidelmel, R. Karim, A. Kaouka, Effects of thermo-mechanical parameters on microstructural and mechanical properties of API X70 steel, *JOM* (2024) 1–8. <https://doi.org/10.1007/s11837-023-06333-0>
- [28] J. Omale, E. Ohaeri, K. M. M. Rahman, J. Szpunar, F. Fateh, M. Arafin, Through-thickness inhomogeneity of texture, microstructure, and mechanical properties after rough and finish rolling treatments in hot-rolled API 5L X70 pipeline steel, *J. Mater. Eng. Perform.* 29 (2020) 8130–8144. <https://doi.org/10.1007/s11665-020-05280-0>
- [29] S. Yadav, T. A. Jack, R. K. Z. Davani, E. Ohaeri, J. Szpunar, Effect of post-processing heat treatment on hydrogen embrittlement susceptibility of API 5L X70 pipeline steel, *Int. J. Pressure Vessels Piping* 199 (2022) 104762. <https://doi.org/10.1016/j.iipvp.2022.104762>
- [30] M. N. Brykov, I. Petryshynets, M. Džupon, Y. A. Kalinin, V. G. Efremenko, N. A. Makarenko, D. Y. Pimenov, F. Kováč, Microstructure and properties of heat affected zone in high-carbon steel after welding with fast cooling in water, *Materials* 13 (2020) 5059. <https://doi.org/10.3390/ma13225059>
- [31] H. Alipooramirabad, A. Paradowska, S. Nafisi, M. Reid, R. Ghomashchi, Post-weld heat treatment of API 5L X70 high strength low alloy steel welds, *Materials* 13 (2020) 5801. <https://doi.org/10.3390/ma13245801>

- [32] O. Hesse, J. Merker, M. Brykov, V. Efremenko, On the strength of low-alloy steels with increased carbon content against abrasive wear, *Tribol. Schmierungstech.* 60 (2013) 37–43. (in German)
- [33] Y. Liu, Y. Tian, X. Wang, Y. Gao, Influence of processing parameters on slab stickers during continuous casting, *High Temp. Mater. Processes* 39 (2020) 228–235. <https://doi.org/10.1515/htmp-2020-0065>
- [34] F. Guo, X. Wang, W. Liu, C. Shang, R. D. K. Misra, H. Wang, C. Peng, The influence of centerline segregation on the mechanical performance and microstructure of X70 pipeline steel, *Steel Res. Int.* 89 (2018) 1800407. <https://doi.org/10.1002/srin.201800407>
- [35] J. Nieto, T. Elías, G. López, G. Campos, F. López, R. Garcia, A. K. De, Effective process design for the production of HIC-resistant line pipe steels, *J. Mater. Eng. Perform.* 22 (2013) 2493–2499. <https://doi.org/10.1007/s11665-013-0544-9>
- [36] E. S. Drexler, A. J. Slifka, R. L. Amaro, N. Barbosa, D. S. Lauria, L. E. Hayden, D. G. Stalheim, Fatigue crack growth rates of API X70 pipeline steel in a pressurized hydrogen gas environment, *Fatigue Fract. Eng. Mater. Struct.* 37 (2014) 517–525. <https://doi.org/10.1111/ffe.12133>
- [37] O. Fyrileiv, O. Aamlid, A. Venås, L. Collberg, Deepwater pipelines-status, challenges and future trends, *Proceedings of Institution of Mechanical Engineers, Proc. Inst. Mech. Eng. M: J. Eng. Marit. Environ.* 227 (2013) 381–395. <https://doi.org/10.1177/1475090212450659>
- [38] T. Tagawa, T. Amano, T. Hiraide, T. Sakimoto, S. Igi, T. Fujishiro, H. Takuya, I. Takehiro, S. Aihara, Inverse fracture in DWTT and brittle crack behavior in large-scale brittle crack arrest test, *J. Pressure Vessel Technol.* 140 (2018) 051205. <https://doi.org/10.1115/1.4040641>
- [39] S. G. Karnaukh, O. E. Markov, V. V. Kukhar, A. A. Shapoval, Classification of steels according to their sensitivity to fracture using a synergetic model, *Int. J. Adv. Manuf. Technol.* 119 (2022) 5277–5287. <https://doi.org/10.1007/s00170-022-08653-y>
- [40] S. Y. Shin, K. J. Woo, B. Hwang, S. Kim, S. Lee, Analysis of fracture toughness in transition temperature region of API X70 and X80 linepipe steels, *J. Kor. Inst. Met. Mater.* 45 (2007) 447–457.
- [41] R. Bruschi, L. Vitali, L. Marchionni, A. Parrella, A. Mancini, Pipe technology and installation equipment for frontier deepwater projects, *Ocean Eng.* 108 (2015) 369–392. <https://doi.org/10.1016/j.oceaneng.2015.08.008>
- [42] A. D. Koval', V. G. Efremenko, M. N. Brykov, M. I. Andrushchenko, R. A. Kulikovskii, A. V. Efremenko, Principles for developing grinding media with increased wear resistance. Part 2. Optimization of steel composition to suit conditions of operation of grinding media, *Journal of Friction and Wear* 33 (2012) 153–159. <https://doi.org/10.3103/S1068366612020079>
- [43] A. Gorni, *Steel Forming and Heat Treating*. Handbook, Socorro SP, 2019. <https://doi.org/10.13140/RG.2.1.1695.9764>
- [44] V. G. Efremenko, D. S. Zotov, V. I. Zurnadzhy, R. A. Kussa, V. I. Savenko, R. I. Sagirov, O. A. Bocharova, A. V. Efremenko, Computer modelling-based selection of accelerated cooling parameters for advanced high-strength structural steel, *IOP Conf. Ser.: Mater. Sci. Eng.* 1037 (2021) 012030. <https://doi.org/10.1088/1757-899X/1037/1/012030>
- [45] H. K. Sung, S. S. Sohn, S. Y. Shin, S. Lee, N. J. Kim, S. H. Chon, J. Y. Yoo, Effects of finish rolling temperature on inverse fracture occurring during drop weight tear test of API X80 pipeline steels, *Mater. Sci. Eng. A* 541 (2012) 181–189. <https://doi.org/10.1016/j.msea.2012.02.019>
- [46] E. B. Mitchell, E. Lucon, L. E. Collins, A. J. Clarke, K. D. Clarke, Microstructure and thickness effects on impact behavior and separation formation in X70 pipeline steel, *JOM* 73 (2021) 1966–1977. <https://doi.org/10.1007/s11837-021-04562-9>
- [47] S. Scholl, A. Schneider, V. Schwinn, Significance of separations occurring in mechanical testing of thermomechanical rolled pipeline steels, *J. Pipeline Sci. Eng.* 2 (2022) 100070. <https://doi.org/10.1016/j.jpse.2022.100070>
- [48] O. P. Ostash, V. V. Panasyuk, I. M. Andreiko, R. V. Chepil, V. V. Kulyk, V. V. Vira, Methods for the construction of the diagrams of fatigue crack-growth rate of materials, *Materials Science* 43 (2007) 479–491. <https://doi.org/10.1007/s11003-007-0056-6>
- [49] D. Stalheim, Recrystallization behaviours in the production of structural steels, 52nd Seminário de Laminiação – Processos e Produtos Laminados e Revestidos, part of the ABM Week (2017) pp. 168–177. ISSN: 2594-5297. <https://doi.org/10.5151/1983-4764-26355>
- [50] L. P. Karjalainen, T. M. Maccagno, J. J. Jonas, Softening and flow stress behaviour of Nb microalloyed steels during hot rolling simulation, *ISIJ Int.* 35 (1995) 1523–1531. <https://doi.org/10.2355/isijinternational.35.1523>
- [51] C. Klinkenberg, K. Hulka, W. Bleck, Niobium carbide precipitation in microalloyed steel, *Steel Res. Int.* 75 (2004) 744–752. <https://doi.org/10.1002/srin.200405837>
- [52] K. Hulka, J. M. Gray, F. Heisterkamp, High temperature thermomechanical processing of pipe-steel, in *Pipeline Technology*, R. Denys (ed.), Elsevier, 2000, pp. 291–306.
- [53] S. Maropoulos, J. D. H. Paul, N. Ridley, Microstructure-property relationships in tempered low alloy Cr-Mo-3·5Ni-V steel, *Mater. Sci. Technol.* 9 (1993) 1014–1020. <https://doi.org/10.1179/mst.1993.9.11.1014>
- [54] T. Gladman, I. D. McIvor, D. Dulieu, Structure-property relationships in high-strength microalloyed steels, In: *Proceedings of the International Symposium on High Strength Alloy Steels “Microalloying’75”*, New York, 1977.
- [55] S. Abraham, R. Bodnar, J. Lonnqvist, J. Hagström, E. Rydgren, The mechanism for coarse Nb-rich particle formation in steel, *Metall. Mater. Trans. A* 52 (2021) 3727–3749. <https://doi.org/10.1007/s11661-021-06324-3>